Merging active and passive data sets in traveltime tomography: The case study of Campi Flegrei caldera (Southern Italy)

Jean Battaglia[1]*, Aldo Zollo[1], Jean Virieux[2] and Dario Dello Iacono[1]

[1]*Dipartimento di Scienze Fisiche, Università degli Studi di Napoli Federico II, Via Coroglio 156, 80124 Naples, Italy, and* [2]*UMR Géosciences Azur, 250 Rue A. Einstein, 06560 Valbonne, France*

ABSTRACT

We propose a strategy for merging both active and passive data sets in linearized tomographic inversion. We illustrate this in the reconstruction of 3D images of a complex volcanic structure, the Campi Flegrei caldera, located in the vicinity of the city of Naples, southern Italy. The caldera is occasionally the site of significant unrests characterized by large ground uplifts and seismicity. The P and S velocity models of the caldera structure are obtained by a tomographic inversion based on travel times recorded during two distinct experiments. The first data set is composed of 606 earthquakes recorded in 1984 and the second set is composed of recordings for 1528 shots produced during the SERAPIS experiment in 2001. The tomographic inversion is performed using an improved method based on an accurate finite-difference traveltime computation and a simultaneous inversion of both velocity models and earthquake locations. In order to determine the adequate inversion parameters and relative data weighting factors, we perform massive synthetic simulations allowing one to merge the two types of data optimally. The proper merging provides high resolution velocity models, which allow one to reliably retrieve velocity anomalies over a large part of the tomography area. The obtained images confirm the presence of a high P velocity ring in the southern part of the bay of Pozzuoli and extends its trace inland as compared to previous results. This annular anomaly represents the buried trace of the rim of the Campi Flegrei caldera. Its shape at 1.5 km depth is in good agreement with the location of hydrothermalized lava inferred by gravimetric data modelling. The Vp/Vs model confirms the presence of two characteristic features. At about 1 km depth a very high Vp/Vs anomaly is observed below the town of Pozzuoli and is interpreted as due to the presence of rocks that contain fluids in the liquid phase. A low Vp/Vs body extending at about 3–4 km depth below a large part of the caldera is interpreted as the top of formations that are enriched in gas under supercritical conditions.

INTRODUCTION

Background

The Campi Flegrei caldera is located west of the city of Naples in a highly populated area. It is a nested calderic system, which is assumed to be mostly the result of two explosive events: the Campanian Ignimbrite eruption (37 ka) and the Neapolitan Tuff eruption (12 ka) (Scandone *et al.* 1991; Orsi, de Vita and Di Vito 1996). The calderic structure contains in its perimeter many craters, mainly monogenic tuff cones and tuff rings, which are the result of more recent eruptions, including the Monte Nuovo which was the site of the last eruption in 1538 (Di Vito *et al.* 1987).

The caldera is strongly affected by bradyseismic activity, which is characterized by large-scale vertical ground

---

*Now at: Laboratoire Magmas et Volcans, Université Blaise Pascal, CNRS, 5, rue Kessler, 63038, Clermont-Ferrand, France. E-mail: battag@opgc.univ-bpclermont.fr

deformations, whose magnitude is unsurpassed anywhere in the world (Newhall and Dzurizin 1988). The two most recent episodes of large and rapid ground uplift occurred in 1970-72 and 1982-84. They led to a cumulative maximum uplift of about 3.5 metres in the town of Pozzuoli (Orsi *et al.* 1999) and were accompanied by swarms of earthquakes and increased degassing. The 1982-1984 bradyseismic crisis led to an uplift of about 1.8 metres (Barberi *et al.* 1984) and was accompanied by more than 15,000 earthquakes. Part of this seismicity is used in the present tomographic study. The bradyseismic crises are superimposed over long-term secular subsidence and since the 1982-84 crisis, the floor of the caldera is subsiding with an average rate of about 5 cm/yr, accompanied by almost no seismicity. Several minor uplift events of a few centimetres, accompanied by swarms of low-magnitude earthquakes, were observed in 1989, 1994 and 2000 (Gaeta *et al.* 2003). Recent results (Troise *et al.* 2007) indicate a renewed ground uplift since November 2004, leading to about 4 cm of uplift up to the end of October 2006.

The source of the bradyseismic activity is still a matter of debate. Two main types of sources have been considered to explain the deformations: the intrusion of new magma into a magma chamber (Berrino *et al.* 1984; Dvorak and Berrino 1991) and the migration of fluid and/or the pressure increase into a hydrothermal reservoir (Bonafede 1991; Bonafede and Mazzanti 1998; Gaeta *et al.* 1998). The second may possibly be caused by a deeper intrusion of magma. A hybrid source involving both hydrothermal and magmatic components has recently been proposed by Gottsmann, Rymer and Berrino (2006). Nevertheless, modelling of ground deformations indicate that any of the possible sources responsible for uplift or subsidence has to be located between 1.5 and 5.5 km depth. The presence of two different sources, with different depths and shapes, has been proposed by Battaglia *et al.* (2006) to explain the uplift and subsidence.

Seismic tomography at Campi Flegrei

Local earthquake tomography is an efficient tool to obtain information on the underground structure of an active area via the assessment of its 3D P and S velocity structures (Aki and Lee 1976; Crosson 1976). The Campi Flegrei caldera has already been the target of several tomographic studies based on various sets of data. Aster and Meyer (1988) used 228 events recorded by a temporary network of the University of Wisconsin-Madison, USA during the end of the 1982–1984 bradyseismic crisis to get both Vp and Vs velocity models.

Vanorio *et al.* (2005) used an upgraded data set composed of 462 events recorded during the same period, with re-picked arrival times for the University of Wisconsin-Madison network complemented with arrival times from the analogue network of the Osservatorio Vesuviano. More recently, data from active experiment SERAPIS have been used by Zollo *et al.* (2003) and Judenherc and Zollo (2004) to obtain P velocity structures of the Bay of Naples and Bay of Pozzuoli. Chiarabba and Moretti (2006) used subsets of both active and passive data sets mentioned previously to obtain Vp and Vp/Vs 3D models of the Bay of Pozzuoli.

The different existing tomographic works provide various velocity models for Campi Flegrei depending on the data set and technique which was used. We propose a strategy for the construction of a unique velocity model which satisfies both passive and active data sets: data from earthquakes recorded in 1984 as well as data from the more recent shots of the SERAPIS experiment. After presenting the different data sets which we used, we examine the effect of merging these sets which have very different characteristics and quantities. We then search for the optimal tomographic parameters and finally present the resolution tests and tomographic results.

DATA

The reconstruction of P and S velocity models of the Campi Flegrei caldera structure is based on a linearized tomographic inversion. Considered traveltimes come from two distinct experiments (Fig. 1).

Passive data

The first data set is composed of 606 earthquakes recorded in 1984 during the end of the last bradyseismic crisis, which occurred in 1982–1984. The events were recorded by a temporary digital network composed of 13 3-component stations, which were installed on 16 sites from mid-January to the end of April 1984. This network was operated by the University of Wisconsin-Madison in collaboration with the Osservatorio Vesuviano to complement the 25 analogue stations operated by the Osservatorio Vesuviano and AGIP (Azienda Generale Italiana). Each digital station recorded data in triggered mode on a stand-alone basis with a sampling frequency of 100 or 200 Hz. The stations were equipped with 3-component 1 Hz Geotech S-13 and Hall-Sears HS-10-1 geophones. Timing was obtained from a 13.6 kHz Omega receiver and the application of a timing-correction process developed for the University
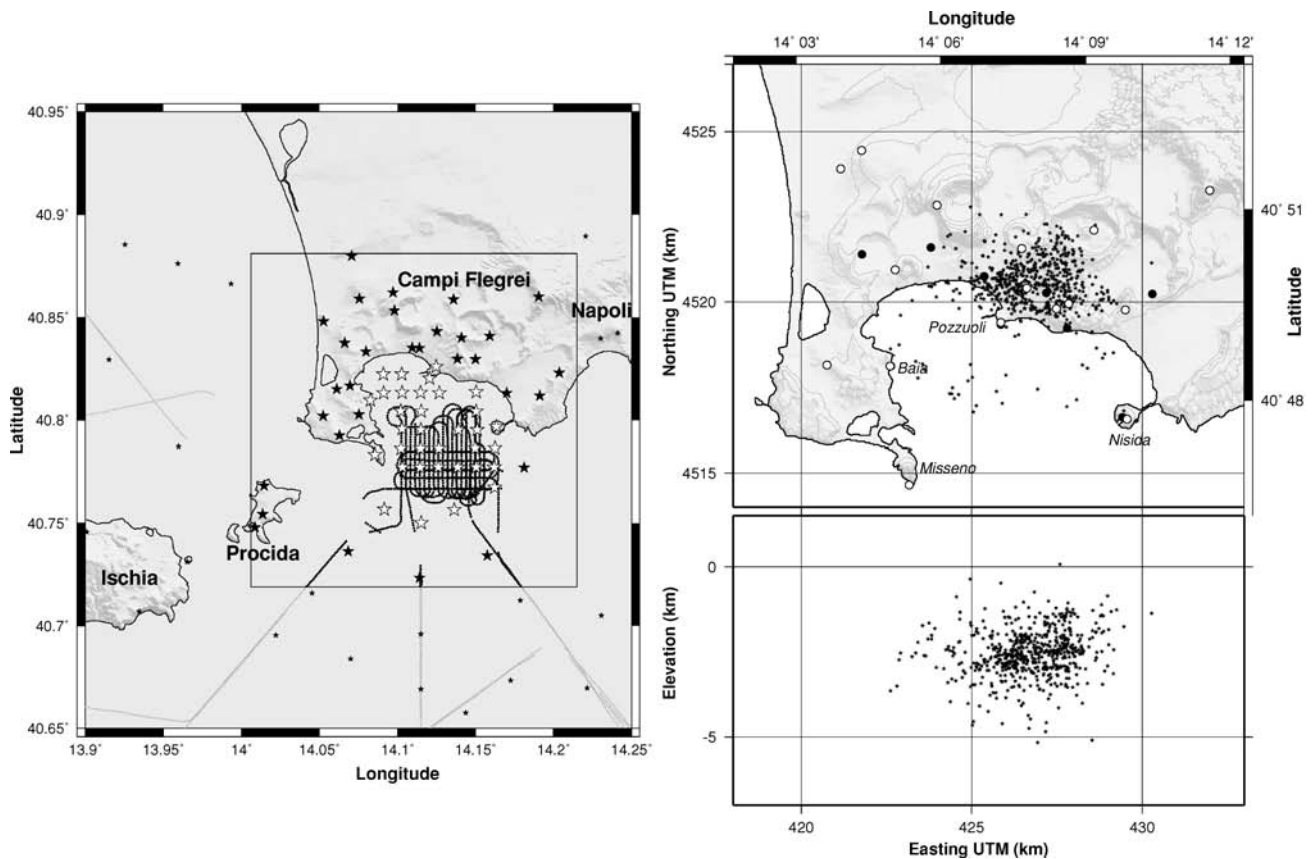
Figure 1 Left: Shaded relief view of the Campi Flegrei caldera and Ischia and Procida islands with the tomography area in the centre. The locations of the shots used for tomography are indicated as black dots and the seismic stations are plotted as stars: empty stars for stations for which precisely re-picked arrival times are available and filled stars for stations for which only preliminary picks are available. The location of the shots outside the tomography area and stations not used in the study are also indicated in a lighter colour. Right: hypocentres of 606 earthquakes recorded during the end of the 1982–1984 bradyseismic crisis and used in this study: map view and east-west cross-section below. The stations used for locating the events are shown as white circles for the stations of the temporary University of Wisconsin-madison network and as black filled circles for the stations of the Osservatorio Vesuviano.

of Winconsin-Madison seismic stations provided a RMS timing error of 1/4 sample relative to Universal Time (Schneider *et al.* 1987). From the records of this network a total of 868 earthquakes have been located, including new events, which became recently available thanks to the retrieval of new data recorded on magnetic tapes. The digital records have been complemented with arrival times from 14 analogue stations of the Osservatorio Vesuviano. Preliminary locations have been obtained using a 1D P velocity model deduced from the tomographic results of Zollo *et al.* (2003). From the available events we selected a subset of 606 well-constrained earthquakes with a minimum of 4 P traveltimes and 3 S traveltimes and and azimuthal gap in station coverage of less than 180 degrees. This passive data set provides a total of 4472 P and 3268 S traveltimes.

Active data

The second data set is composed of recordings for 1528 shots produced during the SERAPIS experiment in September 2001. During the experiment the oceanographic ship Nadir owned by Ifremer fired more than 5000 air-gun shots (Fig. 1). To provide a high density of data in the bay of Pozzuoli, about 2500 shots were fired in the bay along E-W and N-S parallel lines 250 m apart with shots repeated every 125 m along each line. Near the coastline and in the bay of Pozzuoli, the shots were produced by a battery of 6 synchronized air guns, while offshore 12 guns were used. The shots were recorded with 154 stations operated in continuous recording, including 70 sea-bottom receivers and 84 land stations. The sea-bottom receivers were equipped with 4.5 Hz 3-component

sensors and on-land stations included 66 3-component sensors and 18 vertical sensors. The entire experiment produced a total of 700,000 waveforms. A preliminary screening of the traces provided 65,000 P arrivals from sea-bottom stations and 25,000 from on-land stations (Judenherc and Zollo 2004). Later, a subset of the data was reprocessed to improve the quality of the arrival times which provided 36,254 re-picked P traveltimes (Dello Iacono *et al.* submitted). In the present work we only consider a subset of the entire available data set, as we only use the 1,528 shots and 67 stations included in our tomographic area. We merged both picked and re-picked traveltimes, choosing in preference the re-picked ones when available and complementing them with the other ones. Our active data set includes a total of 55,123 traveltimes including 36,195 re-picked and 18,928 picked traveltimes.

THE TOMOGRAPHIC INVERSION PROCEDURE

The tomographic inversion is done using an improved method based on an accurate traveltime calculation using the finite difference computation scheme of Podvin and Lecomte (1991). Three dimensional P and S velocity models are obtained by inverting P and S first arrival times simultaneously for both velocity models and earthquake locations (Thurber 1992). The procedure is iterative and at each iteration a linearized inversion of delayed traveltimes is performed as proposed by many authors (e.g. Aki and Lee 1976; Spakman and Nolet 1988; Benz *et al.* 1996). The inversion is done with P and S velocity models parametrized as 3D grids of regularly spaced nodes. According to our station/source configuration, we consider in this work a tomographic volume of 18*18*9 km starting 0.5 km above sea level (Fig. 1) with a node spacing of 0.5 km in all directions. Each iteration can be subdivided into 4 main stages: (1) interpolation of the velocity models into finer grids and calculation of the theoretical traveltimes, (2) calculation of derivatives, (3) preconditioning and smoothing of the derivative matrix and (4) inversion by means of the LSQR method (Paige and Saunders 1982).

The forward problem of traveltime computation is done by solving the Eikonal equation with a finite differences algorithm. For this calculation fine P and S grids of constant slowness cells are required and such models are obtained by trilinear interpolation of the tomographic inversion grids. In the present case we use fine grids with a spacing of 0.1 km in all directions. The finite difference scheme of Podvin and Lecomte (1991) is well suited for the calculation of precise

traveltimes in highly heterogeneous media with large velocity contrasts. It allows for each station to obtain a first estimation of the traveltimes at each node of the fine grid. It is then possible to trace back rays for each station-source pair by following the gradient of the estimated traveltimes. Finally, precise traveltimes are calculated by integration of the slowness along the traced rays. Latorre *et al.* (2004) showed that this computation improves the precision of the calculated traveltimes as compared to those calculated by wavefront reconstruction.

Traveltime partial derivatives are computed simultaneously for P and S slowness fields, hypocentre locations and origin times of earthquakes (Le Meur, Virieux and Podvin 1997). Normalization and scaling of the derivative matrix is performed to control the quality of the retrieved parameters. To ensure numerical stability and to control the degree of model roughness, the system is preconditioned and smoothed. The smoothing is achieved by requiring that the Laplacian of the slowness field must vanish (Benz *et al.* 1996). The degree of smoothing in the different directions is defined using parameters Lx, Ly and Lz, whose values are discussed later in this paper. The quality of the different observations is taken into account by weighting the different traveltimes. Initial weighting of the different data was done as follows: for earthquakes we assigned weights of 1.0, 0.5, 0.2 and 0.1 for picked arrival times with respective quality (hypo71 software; Lee and Lahr 1975) 0, 1, 2 and 3 and for shots, we assigned a weight of 1.0 for precisely re-picked shots and 0.6 for preliminarily picked shots. Changes in the relative weighting of the different data sets are discussed later by means of synthetic tests and tomographic runs. Finally, the inversion of the scaled and weighted linear system was done using the LSQR algorithm (Page and Saunders 1982). The inversion was regularized using a damping factor whose optimal value is discussed later.

MERGING OF THE TWO SETS OF DATA

The joint inversion problem is especially difficult since the active and passive data sets are complementary: the first one provides both Vp and Vs velocity models, as well as earthquake locations but has a lower resolution and a limited spatial coverage, while the second has a higher resolution but only provides P velocity and samples mostly shallow layers. Figure 2 shows the ray coverage provided by each set and emphasizes that the two sets overlap only over a limited area. We also note that the amounts of rays provided by each set are very different.
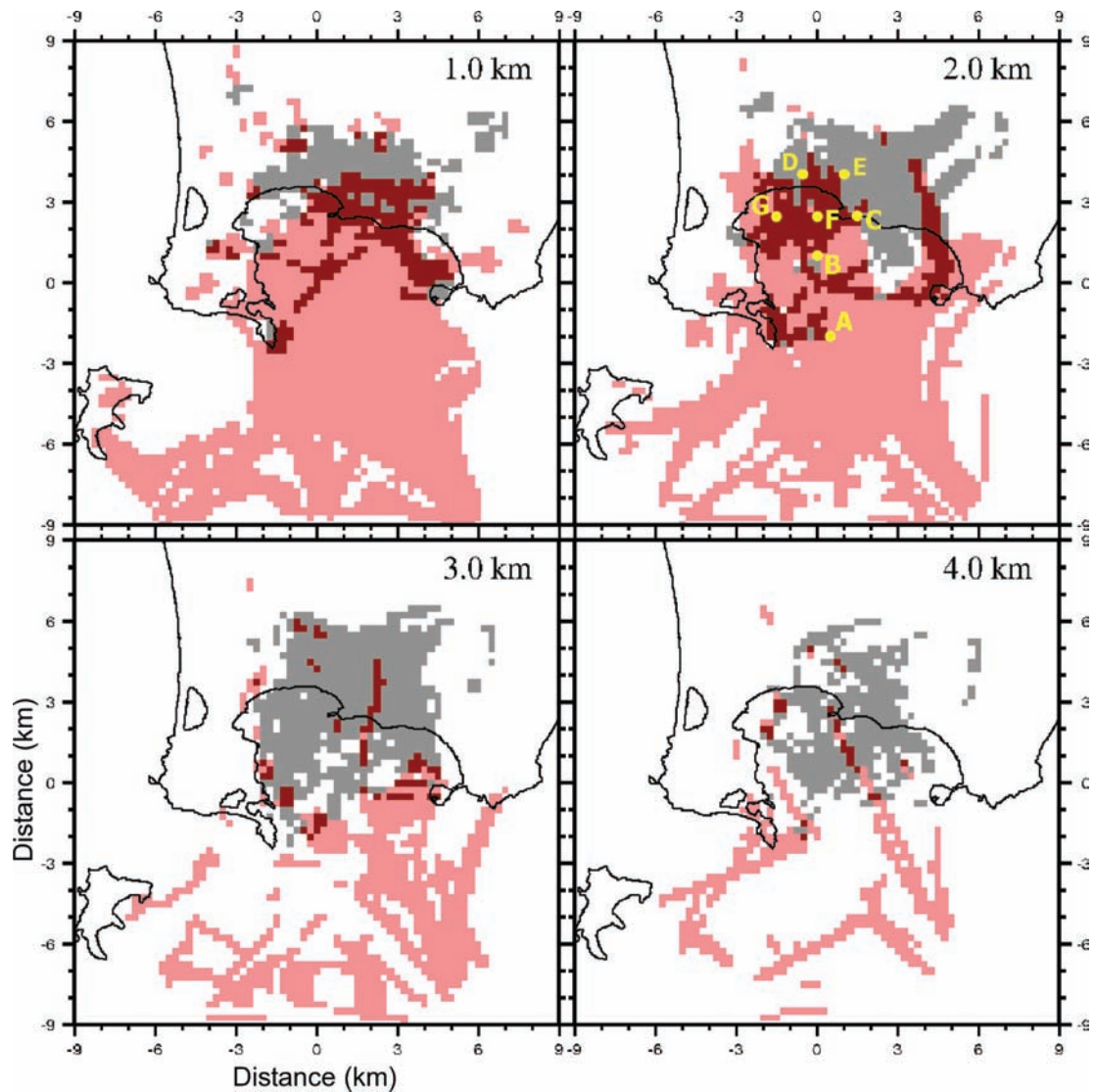
Figure 2 Horizontal cross-sections showing the cells crossed by rays at different depths of the tomography grid (1, 2, 3 and 4 km depth). Cells crossed by rays from shots are in pink, those crossed by rays from earthquakes are in grey and those crossed by rays from both types of data are in red. Epicentral locations where spike tests have been performed to determine the effect of merging the data sets are indicated on the cross-section at 2 km depth.

Effect of merging the sets

To examine the effect of merging the two data sets we performed some spike tests at different epicentral locations of the grid (noted A to F in Fig. 2) and at different depths. These local-scale tests are particularly interesting as they provide an insight into the resolution matrix. Each spike test is done by (1) adding to a smooth 1D initial velocity model a 500 m/s anomaly with a width of 1 km at half the peak amplitude, (2) calculating synthetic traveltimes for the chosen event/station

configuration and (3) inverting the synthetic traveltimes starting from the original velocity model and using the same inversion parameters and grid settings as for tomography. From a general point of view, we note that on any point of the grid the restitution of a spike with a 500 m/s amplitude is better than for a spike with a lower amplitude and that the quality of the restitution is independent of the sign of the anomaly.

At each point and depth, we made spike tests considering three combinations of data (keeping weights at their initial
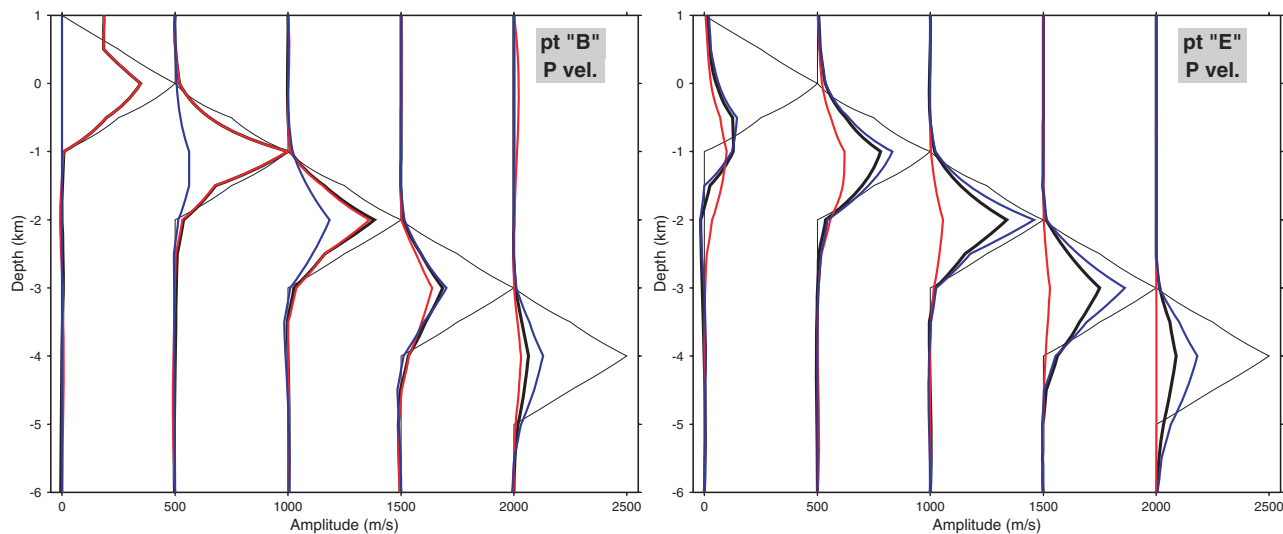
Figure 3 Comparison between spike restitutions for P waves at points B and E when using shots only (red), earthquakes only (blue) and both (thick black). The spike initially introduced is shown as a thin black line.

values): only earthquakes, only shots and both shots and earthquakes. For P waves, three main situations emerge from the tests depending on spike location: spike restitution provided by earthquakes is better than the one provided by shots, worse or equivalent. To illustrate the first two cases, Fig. 3 shows results for P-wave spike tests at points B and E for the three combinations of data. At point B, at shallow depth the resolution is high and mostly comes from the shots, while deeper it comes from the earthquakes and is low due to the low ray coverage. At point E, the resolution mostly comes from the earthquakes and is high down to 3 kilometres. These plots emphasize that in areas where earthquakes are dominant, the joint inversion leads to a loss in resolution since spike reconstitution is lower than the one obtained when using only earthquakes. In areas dominated by shots the resolution remains unchanged when merging as compared to shots only, even if the resolution of the earthquakes is low. In a few locations, the resolution with the merged data set is a little better than the resolution with any of the individual sets but this effect is limited. For S waves, the resolution comes entirely from the earthquakes and the addition of shots has a very limited impact. A slight increase of the resolution is observed with the merged set, mostly at shallow depth and a very small reduction, mostly in deeper areas.

Solutions for improving the resolution

A first class of solutions to correct for the loss of resolution is to adjust the weights of the different sets of traveltimes. Due to the weighting scheme used in our program, down-weighting the shots does not provide an adequate solution as it increases the influence of the starting velocity model and does not allow the inversion to converge toward a low residual for the shots. Practically, this leads to the disappearance of the tomographic image provided by the shots. An adequate solution to compensate for the loss of resolution is to increase the weight of the earthquakes. Figure 4 shows a comparison of spike restitutions for three combinations of data: both shots and earthquakes alone and shots and earthquakes with the weight of earthquakes multiplied by a factor of 2. This solution allows one to regain the original resolution provided by the earthquakes or to improve it. Similarly such a weight increase for S waves improves spike restitution. We note however, that the effect on tomography of increasing the weights is to increase the amplitude of velocity anomalies and excessive over-weighting introduces small wavelength and high amplitude anomalies, providing unstable tomographic images.

An alternate solution that allows one to avoid the loss of resolution is to reduce the amounts of shots. Since the shots are regularly spaced along the boat tracks, this can easily be achieved by only considering every second or fifth shot for example. Figure 5 shows a comparison between spikes reconstructed using data sets with different amounts of shots, it emphasizes that reducing the quantity of shots increases the effect of earthquakes and allows one to better restore spikes in areas where resolution is mostly provided by earthquakes (point E). This reduction, even by a factor of five, does not significantly lower the resolution provided by shots when their
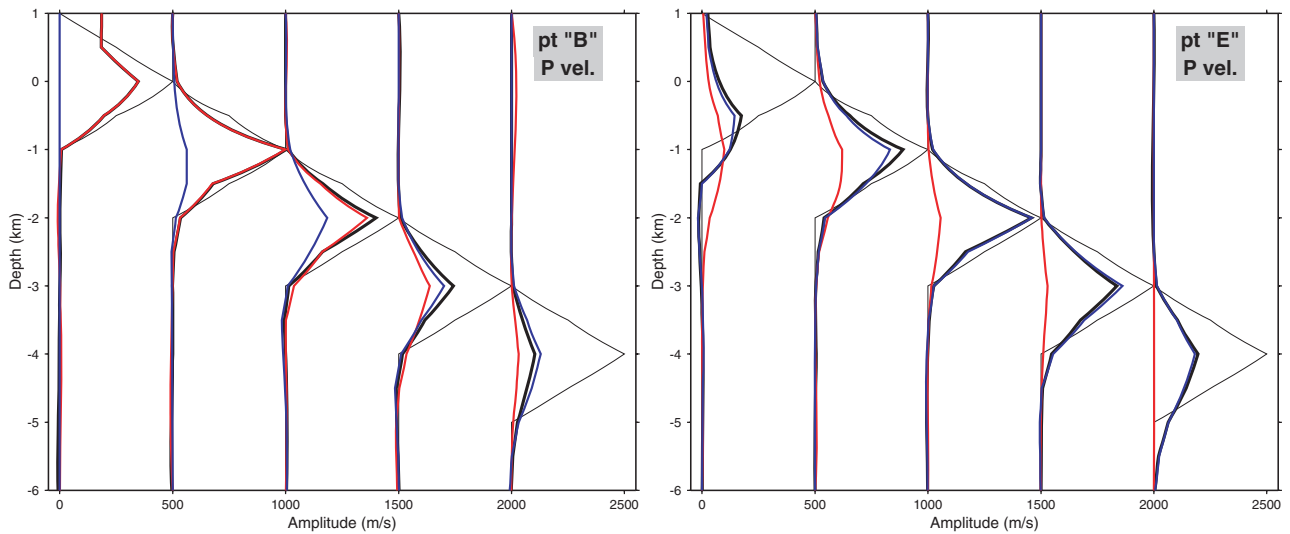
Figure 4 Comparison between spike restitutions for P waves at points B and E when using shots only (red), earthquakes only (blue) and both with earthquakes weights multiplied by 2 (thick black). The spike initially introduced is shown as a thin black line.
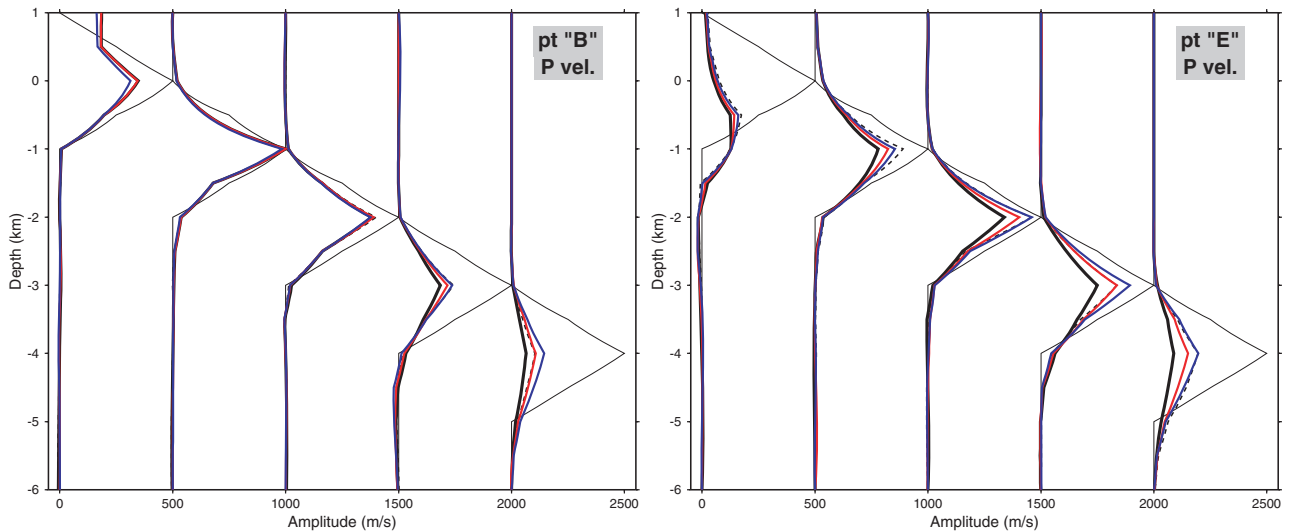

Figure 5 Comparison between spike restitutions for P waves at points B and E when using earthquakes and various amounts of shots: all (thick black), only 50 percent and only 20 percent (blue). The restitutions when using all shots and earthquakes with weights multiplied by 2 are also shown (dashed black). The spike initially introduced appears as a thin black line.

effect is dominant (point B). However, we note that the effect of reducing the amounts of shots is to reduce the ability to reconstruct larger scale anomalies, as shown later by doing larger scale 'shape tests'.

INVERSION SETTINGS

While spike tests provide insights into the effect of merging the two data sets, as well as possible solutions to compensate for the observed loss of resolution, larger scale synthetic tests, as well as real tomographic runs are required to determine the optimal parameters to use in the tomography. For this purpose we proceed with synthetic tests, in which larger scale velocity anomalies with various shapes are introduced ('shape tests'). These tests are done as a 3-stage process, similarly to the previous spike tests. We note that in these tests, the location of the earthquakes is not kept fixed as opposed to the resolution tests presented later. We also carried out various tomographic runs to examine the complexity of the obtained tomographic images depending on the parameters.
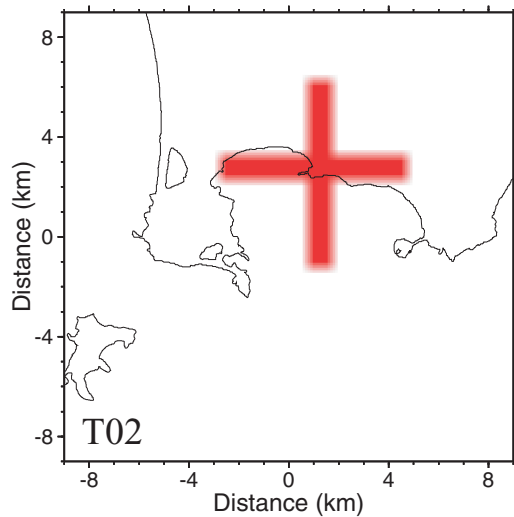
Figure 6 Shape of the input anomaly for test T02, P and S waves (shapes for tests T01 and T03 are shown in Fig. 9).

Once the size of the inversion cells is fixed, the main parameters that have an influence on the tomographic results are the smoothing coefficients Lx, Ly and Lz, which control the preconditioning of the matrix of traveltime delays, the damping factor DAMP, which regulates the LSQR inversion and, in the present case, the increase in the weight of the earthquakes (P and S waves) and the amounts of shots that we used. In the present work, we consider homogeneous smoothing in all directions and take the same value for Lx, Ly and Lz, which we note LX later on. To determine the proper parameters to use for tomography, we first compare the quality of recomposed synthetic anomalies when using different values. We present here results for three different shape tests that cover various areas of the tomographic grid:

- Test T01: an annular anomaly with a 100 m/s amplitude added at each depth in the periphery of the tomography grid to the P velocity model (Fig. 9).
- Test T02: a 100 m/s anomaly shaped like a cross added in the centre of the grid at each depth to both P and S velocity models (Fig. 6).
- Test T03: two annular anomalies with opposite signs added at each depth. For the P model, the internal anomaly is +150 m/s and the external −200 m/s; for the S model, the inside anomaly is −150 m/s and external +200 m/s (Fig. 9).

To simplify the analysis of the results, we represent each synthetic test by its average error, which is defined as the average of the absolute value of the difference between the introduced and the reproduced anomaly. This error is calculated over all the nodes between 0 and 4 km below sea level, which is the best resolved part of grid. We normalize the obtained values to the average amount of anomaly introduced initially. Figure 7 shows results obtained for tests T01 and T02 for various values of the damping and for various multiplicative factors applied to the weight of the earthquakes. The results suggest that appropriate values for damping are in the range between 0.3 and 0.5. The choice of the multiplicative factor for the weight of the earthquakes is more problematic, as its effect appears to depend on the location of the anomaly: for P waves, increasing the weights increases the mean error for test T01 and decreases it significantly for test T02. A satisfactory compromise for P waves is found by multiplying the weight of earthquakes by two, as this also compensates for the loss in resolution caused by data merging. For S waves, synthetic tests suggest a better reproduction of the anomalies with increasing weight without providing an uppermost boundary for the value to use.
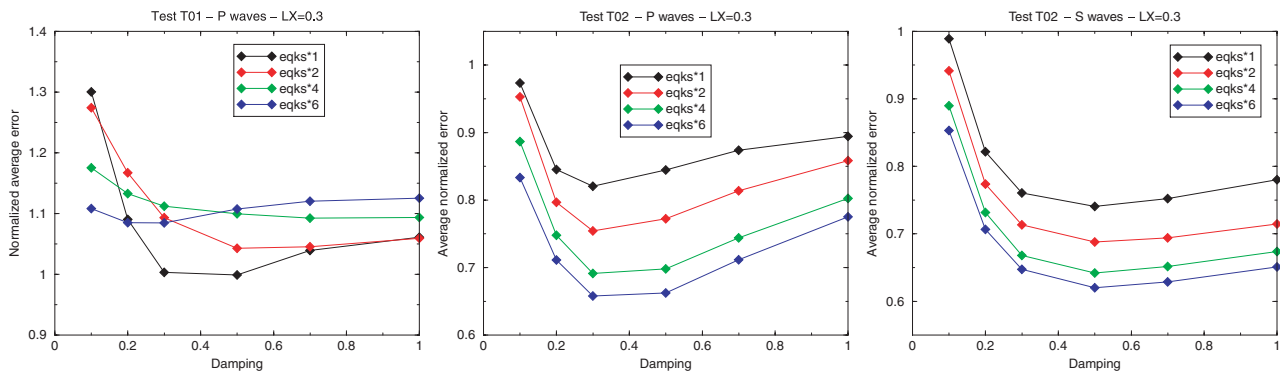
Figure 7 Mean error rates for test T01 P waves and test T02 P and S waves as a function of the damping. Each symbol represents the average of the absolute value of the difference between the introduced velocity anomaly and the one restored. This average is calculated over all nodes between 0 and 4 km b.s.l..

To help constraining the choice of the P and S multiplicative factors, we take into account another criterion which is the simplicity of the obtained velocity models when doing the tomography. Indeed, a major effect of increasing the weight of the earthquakes (P and S waves) is to increase the complexity of the obtained velocity models by introducing higher amplitude, small wavelength anomalies. It is well known that in tomography it is generally possible to find a whole class of models, instead of a single model, which fits equally well the observations (Monteiller *et al.* 2005). The choice of the best model in that class is done by choosing the result with the lower degree of freedom (Akaike 1974; Tarantola and Valette 1982). For this purpose we examine the variance of the P and S velocity models and Vp/Vs ratio obtained with various multiplicative factors and examine the corresponding residuals for P and S traveltimes. For P-waves, results indicate that a good choice is found with weights multiplied by two, which is in good agreement with results suggested by the above synthetic tests. For S-waves, however, increasing weights leads to a reduction of the individual rms for S-waves in general but also to an increase of the variance of the Vp/Vs model in particular. Solutions that do not imply a substantial increase of the variance for the final velocity models are found for S-weights multiplied by up to 4.

In a similar way to Fig. 7, Fig. 8 shows the effect of reducing the amounts of shots. Despite the fact that such a reduction allows one to avoid the loss of resolution according to spike tests, the results for shape tests indicate that it leads to a significant reduction in the ability to reproduce anomalies in the peripheral area of the grid (test T01), where the resolution comes mostly from the shots. For more central anomalies (test T02), the reduction leads to few changes. In general, however, the effect of increasing the earthquakes weight by a factor of two brings significantly better results. Combining earthquakes weight increase and reduction of shots leads to inappropriate solutions in a similar way to over-weighting the earthquakes. This indicates that the weight increase is only permitted by the stabilizing effect brought about by the large amount of shots traveltimes.

Finally, to determine a proper value to use for the smoothing coefficients we proceed with visual inspections of the recomposed anomalies. Figure 9 shows results for tests with various values of LX. The images indicate that appropriate values for LX are in the range 0.2 to 0.3. Lower values lead to the appearance of small-scale asperities and larger values provide blurred images.

RESOLUTION TESTS

In order to identify the well resolved areas of the tomographic images, we performed several synthetic tests on a global scale (checkerboard and shape tests) as well as on a local scale (spike tests). All tests are done in a similar way to the tests used to determine the effect of merging the passive and active data sets, except that the position of the sources is kept constant during the inversion of synthetic traveltimes. Tests are carried out with the same station-event configuration as for tomography and with the same inversion parameters and grid settings (grid size, origin and spacing).

Checkerboard test

A checkerboard test was first performed to obtain a global view of the resolution for both P and S waves. This test is done by adding a grid of positive and negative anomalies with sizes of 2 km in all directions and with an amplitude of ±50 m/s to simple one dimension P and S velocity models. Figure 10 shows the restitution of the anomalies with areas not sampled by any ray shown in lighter colours. The test indicates that
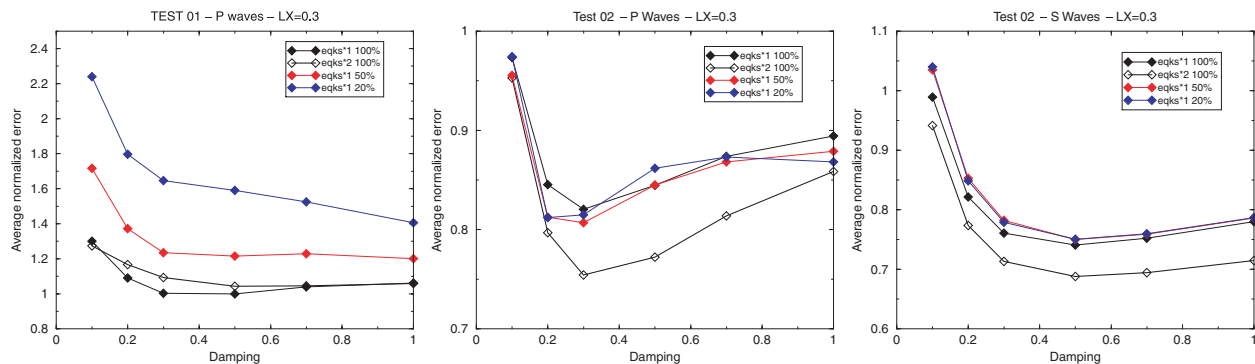
Figure 8 Mean error rates for test T01 P waves and test T02 P and S waves as a function of the damping when taking into account various quantities of shots. Each symbol represents the average error calculated over all nodes between 0 and 4 km b.s.l..
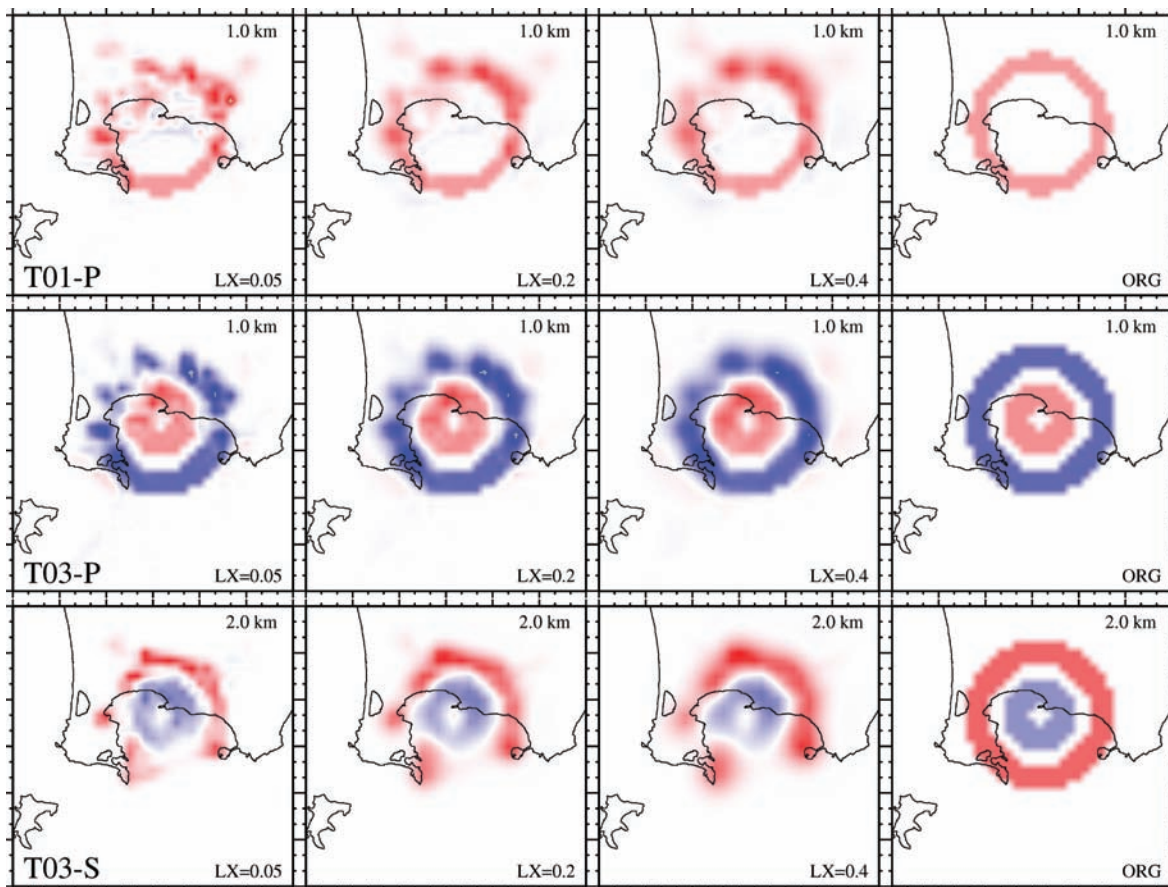
Figure 9 Restitution of velocity anomalies for tests T01 (P waves, upper plot) and T03 (P and S waves, middle and lower plot) for LX = 0.05, LX = 0.2 and LX = 0.4. Original anomalies are on the right. For all plots, the anomalies are superposed to the same tomographic area as in Fig. 2, which is 18*18 km.

for P waves the resolution is optimal at 1.5 km depth where a good restitution of anomalies is obtained for a large part of the tomography grid. At 0.5 km depth the resolution remains very good below the whole bay of Pozzuoli, with still reasonably reconstructed cells below the northern limit of the bay. More than 2 km below sea level (b.s.l.) some smearing starts to appear due to rays traveling in single directions. For S waves, the checkerboard pattern is well reconstructed for cells below and around the town of Pozzuoli from about 1.5 km b.s.l. down to 3.5 km b.s.l.. For the shallow layer at 0.5 km b.s.l. the reconstruction is poor.

Spike tests

To obtain an insight into the resolution matrix of the tomographic grid, local scale synthetic tests were performed at different nodes of the grid. Such tests are done by adding to simple 1D P and S velocity models, at a single point of the

grid, an anomaly with a 500 m/s amplitude and with a width of 1 km at its half amplitude. The process is repeated at 4 different depths and various epicentral locations with a total of 440 tests done. Results of the reconstructed P and S spikes are represented in Fig. 11, in which at each depth the spikes, represented along vertical profiles, are shown in the epicentral position at which they were introduced. We note that in general the restitution of negative spikes is similar to positive ones and that larger amplitude anomalies (500 m/s) tend to be better reconstructed than smaller anomalies (100 m/s). Results confirm the well resolved areas of the grid indicated by the checkerboard test and show that the restitution of both P and S amplitudes is very good in those areas.

Shape tests

Finally, several shape tests similar to those used to determine the proper inversion parameters were carried to determine the
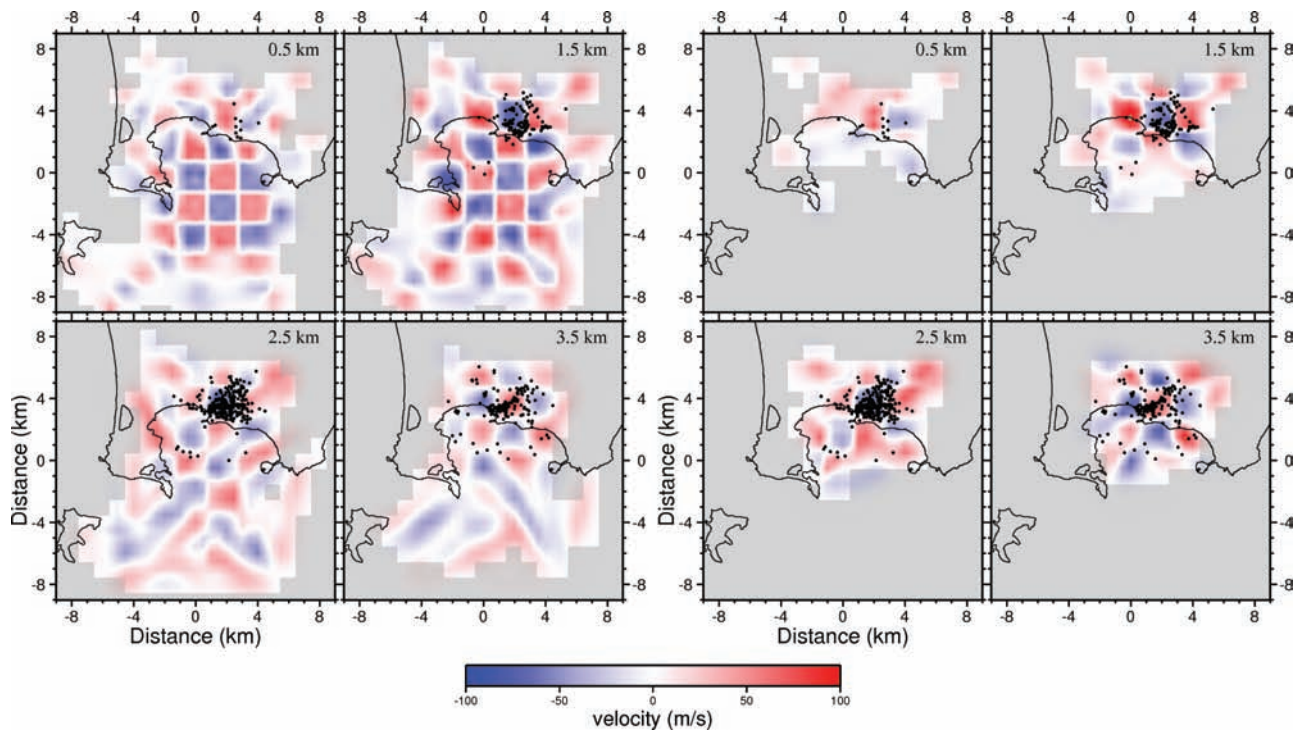
Figure 10 Results for a checkerboard test with 2*2*2 km cells with ±50 m/s anomalies added to P (left) and S (right) velocities.

ability of our station/event distribution to enlighten particular features such as those appearing in the final tomographic result. In particular, we proceeded with a test T01b, similar to test T01, in which in addition to a cylindrical velocity anomaly added to a smooth P velocity model, a Vp/Vs anomaly was added so that the Vp/Vs ratio decreases with depth. The purpose of this test was to examine first the ability of the technique to identify the presence of the caldera rim in the peripheral areas of the grid as well as a steady change of the Vp/Vs ratio with depth. Figure 12 shows results for this test presented as horizontal sections of the P anomaly and vertical profiles of the Vp/Vs ratio. We note that the reproduction of a negative P anomaly is as good as for a positive anomaly and that the reproduction of a decreasing or increasing Vp/Vs ratio is equivalent. The results indicate that a good reproduction of the introduced P anomaly can be obtained at shallow depth down to 2 km b.s.l. At 3 km b.s.l. the pattern is still reproduced while it becomes blurred and at 4 km b.s.l. the pattern almost disappears because of the low ray coverage. Vertical profiles of the Vp/Vs ratio show that below the town of Pozzuoli (x = 1, y = 2.5) as well as below the Solfatara (x = 2.5, y = 2.5) the reproduction of the Vp/Vs anomaly is good from about 0.5 to 4.5 km b.s.l.. At very shallow depth, the technique is unable to properly reproduce variations in the Vp/Vs ratio. Results for

tests T02 and T03 confirm the good restitution of cylindrical or linear patterns down to 2–3 km in the central portion of the grid.

TOMOGRAPHY RESULTS

We present tomographic results obtained with DAMP = 0.5, LX = 0.3, using all available shots and with the weight of earthquakes multiplied by two for both P and S waves. Other values in the range defined by the synthetic tests discussed previously provide comparable results and the features we describe below are stable.

The tomography technique we used is an iterative, linearized and perturbative technique, which implies that the final velocity model may depend on the chosen initial model (Kissling *et al.* 1994). The choice of the initial 1D model was done in two steps. First, the 1D model chosen for Campi Flegrei caldera by Vanorio *et al.* (2005) was used as a starting model to process a first tomographic run. In a second rune, the P and S resulting velocity models were used to calculate average vertical velocity profiles for both P and S waves. The averaging was done by stacking a large number of profiles extracted in the resolved parts of the tomographic grid. The obtained profiles were used as initial models. We note, however, that
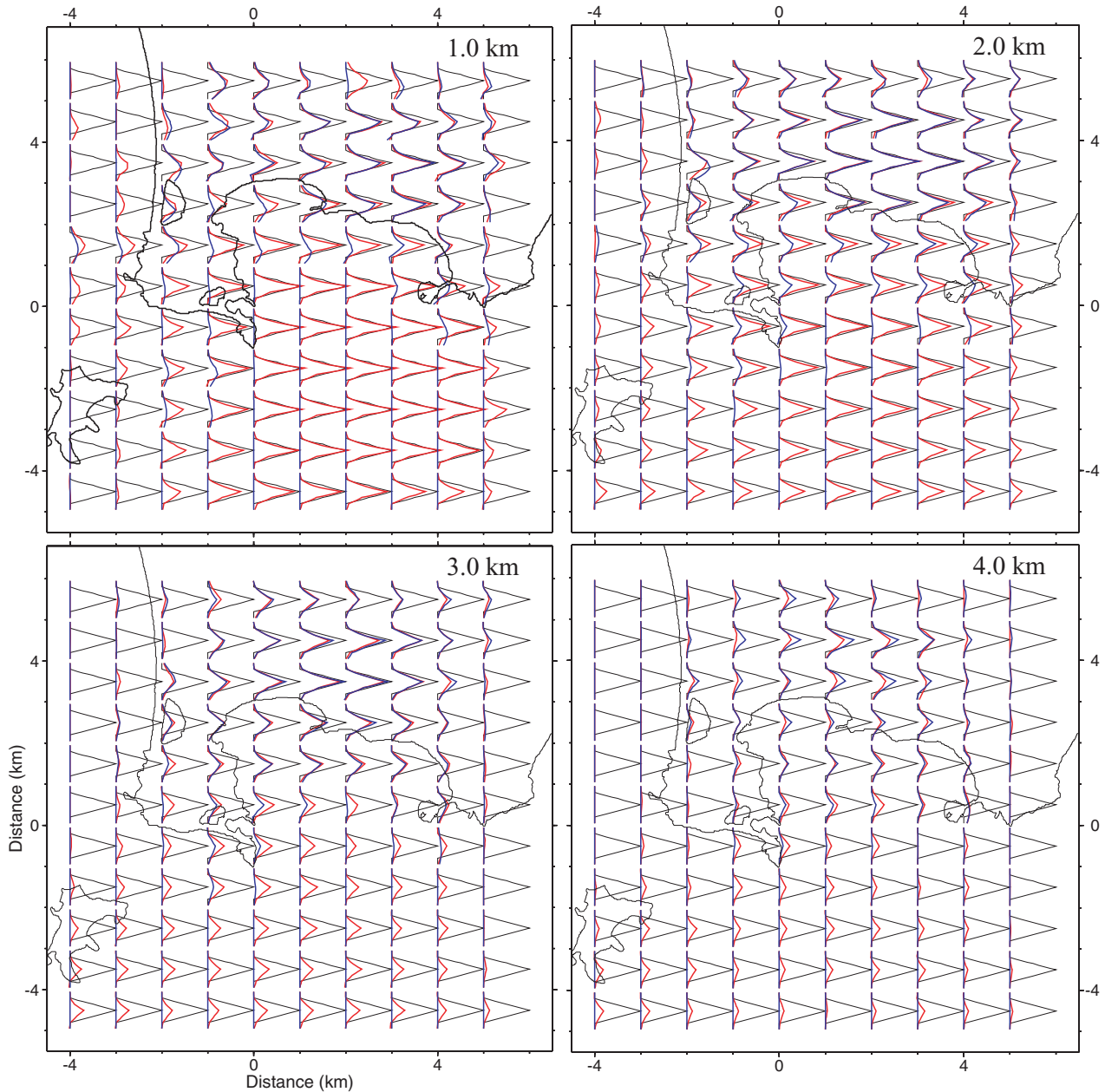
Figure 11 Restitution of spike tests for P and S waves at different locations and depths of the tomography grid. Each spike test was done individually by adding at a single point of the grid an anomaly with a 500 m/s amplitude and a width of 1 km at its half amplitude. Results are represented as vertical anomaly profiles at the node where the anomaly was introduced. The introduced anomalies are represented as thin black lines (same amplitude for P and S waves), the reconstructed anomalies for P waves are in red and for S waves in blue. Spikes are scaled to avoid overlapping.

most of the features discussed below are not very sensitive to the choice of the initial model.

The iterative process is stopped after 15 iterations, while most of the rms residual reduction is achieved in the first five iterations. The process drops the total rms from about 0.15 to 0.07. Residuals calculated independently for active and passive data sets are very similar to values which are obtained when doing tomography with each set individually. This indicates that there is no major incompatibility of the two sets such that adjusting one set would prevent fitting of the other
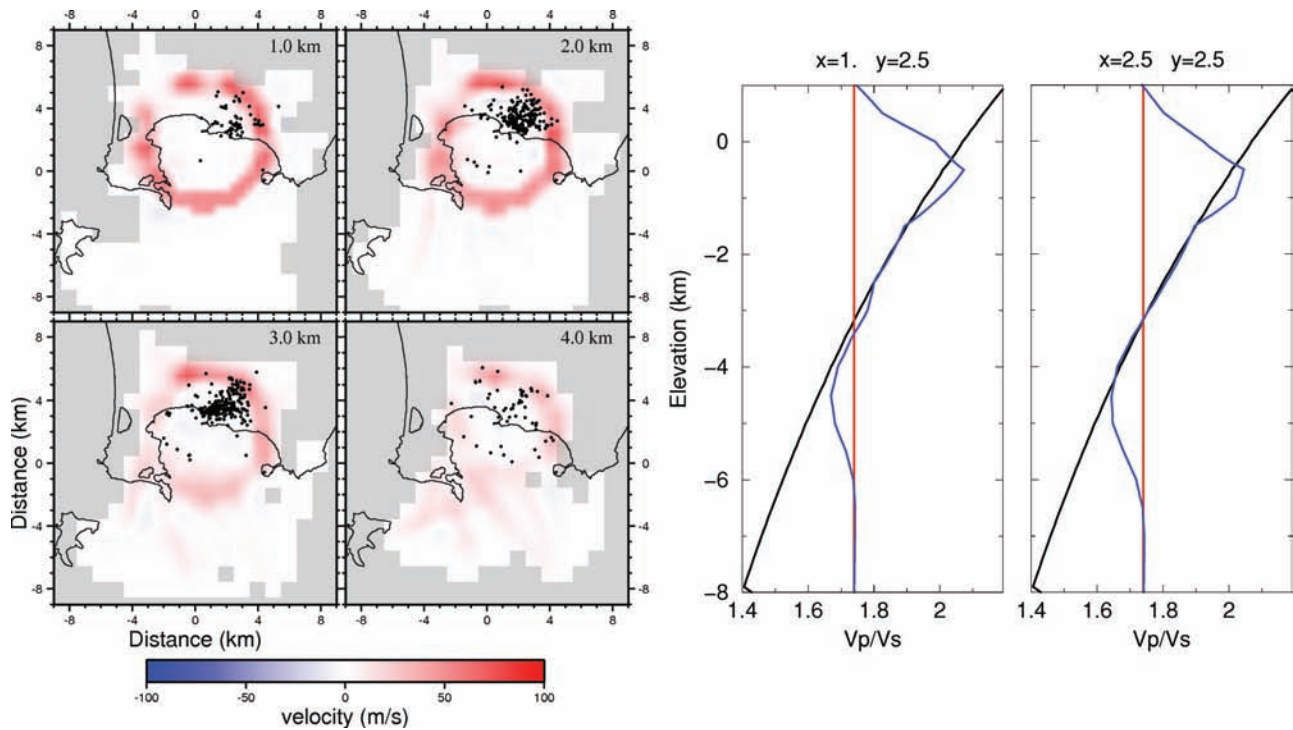
Figure 12 Results for synthetic test T01b showing the reconstruction of the P anomaly at different depths (left) and 2 vertical profiles showing the reconstruction (blue) of the Vp/Vs anomaly (black).

one. The obtained 3D velocity models, as well as earthquakes locations are shown in Figs 13 to 15. Cells not sampled by any ray are shown in lighter colours.

P velocity model

Figure 13 shows the obtained final P velocity model presented as horizontal cross-sections. The most characteristic feature that emerges is the presence of a ring-shaped high P velocity anomaly, which is particularly clear around 1.5 km b.s.l.. Our results confirm the presence of this ring in the southern part of the bay of Pozzuoli, as previously observed by Zollo *et al.* (2003) and Judenherc and Zollo (2004) but also extend its trace inland along the western border of the bay and less clearly along the eastern border below and north of the island of Nisida. At 1.5 km depth, no clear trace of the ring continuation is observed in the northern part of the grid, while synthetic tests suggests an annular anomaly could be reconstructed there if present in the resolved part of the tomography area (Fig. 12). The structure which is defined by our results has a diameter of about 8–12 km at 1.5 b.s.l.. We note that at this depth, the shape of the ring is in good agreement with the location of hydrothermalized lava inferred by gravimet-

ric data modeling (Fig. 16). In total, the trace of the ring can be seen from about 0.5 km b.s.l. down to about 2.5–3.0 km. At 3 km depth its trace is, however, less clear and appears as a lower velocity zone surrounded by higher velocity structures, including on the northern side, with a diameter of about 6 km.

Vp/Vs model

The obtained Vp/Vs model presents several interesting features (Figures 14 and 15). The Vp/Vs East-West cross section at y = 2.5 (Fig. 14), which passes below the town of Pozzuoli, outlines the presence of a very high Vp/Vs anomaly located at about 1 km b.s.l. below the town as observed previously by Aster and Meyer (1988) and Vanorio *et al.* (2005). This anomaly has values up to 2.7, with a lateral extent of about 1 to 2 km. According to synthetic tests, the uppermost extent of the anomaly is poorly constrained and near the surface the ratio depends strongly on the value of the initial velocity model. We also note an extension of the high Vp/Vs anomaly toward the Solfatara area (horizontal cross-section at 2 km depth in Fig. 15). The amplitude and size of this secondary anomaly is sensitive to the weight of the S waves used in the
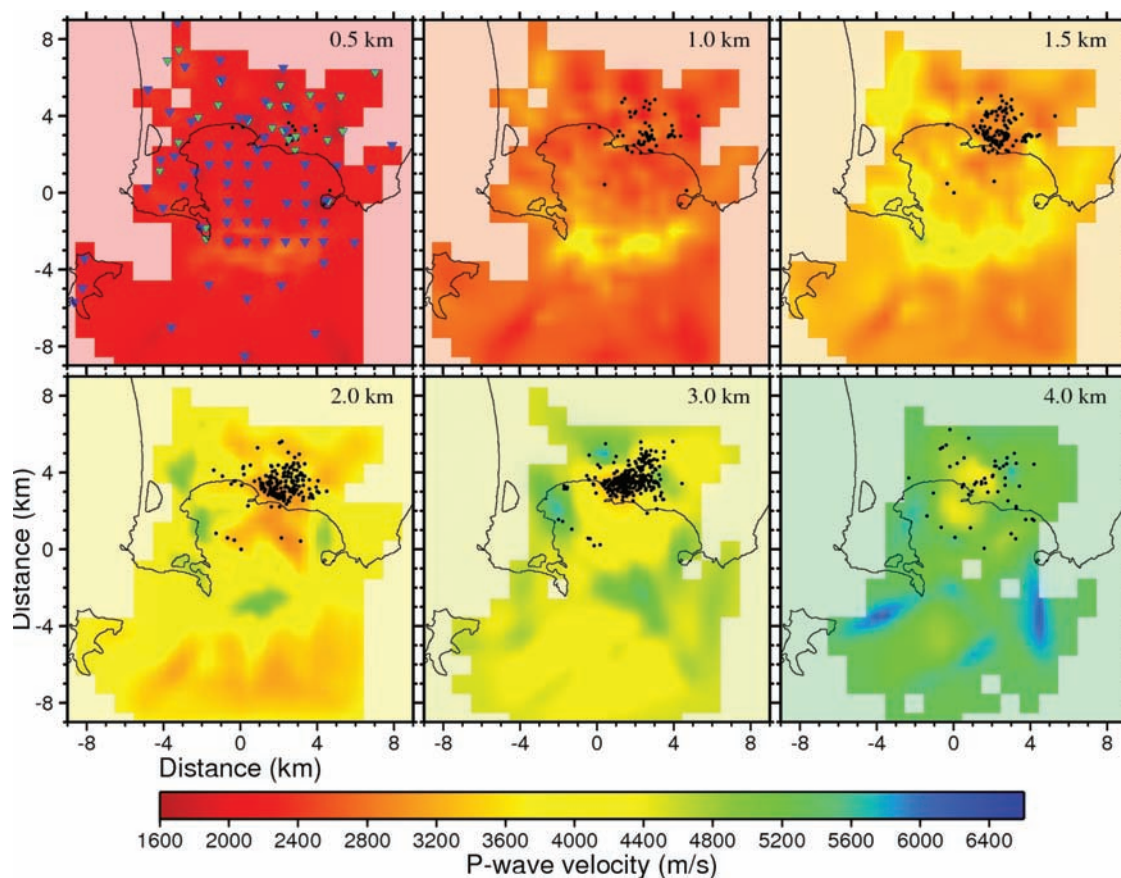
Figure 13 Tomography results: horizontal sections of the P velocity model.

inversion. The results presented in this paper favour the choice of a smooth Vp/Vs model by using S weights multiplied by a factor of 2 while the use of a factor of 4 tends to increase the roughness of the model and increases the size and amplitude of this anomaly. Horizontal cross-sections of the Vp/Vs ratio (Fig. 15) confirm the presence of a low Vp/Vs body extending at about 3–4 km depth below a large part of the caldera with values down to 1.3–1.4. The upper limit of this structure however, is not smooth according to the vertical cross-section in Fig. 14.

Earthquake locations

Finally, looking at the position of the relocated earthquakes in the 3D final velocity structure, we note that the events appear generally more clustered than according to the initial locations. Horizontal cross-sections (Fig. 13) show that most of the events found inland below the Pozzuoli area are roughly aligned along an SW-NE elongated pattern, most clear at about 3 km depth. Most of the seismicity is found at the upper limit

and above the low Vp/Vs body located at about 3–4 km depth. We also note an interesting feature that appears on the vertical cross-section in Fig. 15, which shows that the earthquakes define a 45 degree dipping plane below which most of them are found and above which is located the high Vp/Vs shallow anomaly.

DISCUSSION

Our tomographic results outline several characteristic features that can be interpreted in terms of the previous studies done in the Campi Flegrei area. Previous results obtained from gravimetric, seismic activity, and drilled-rock sampling analyses conducted in Pozzuoli Bay and on land have been used for geological interpretation of Vp and Vp/Vs anomalies on the basis that the P and S velocity distribution and their Vp/Vs ratio can be associated with the elastic characteristics of rocks under investigation and with the physic state of the pore fluid.

By analysing the horizontal sections of the P-velocity model in Fig. 13, we observe at about 1 km depth an arc-like positive
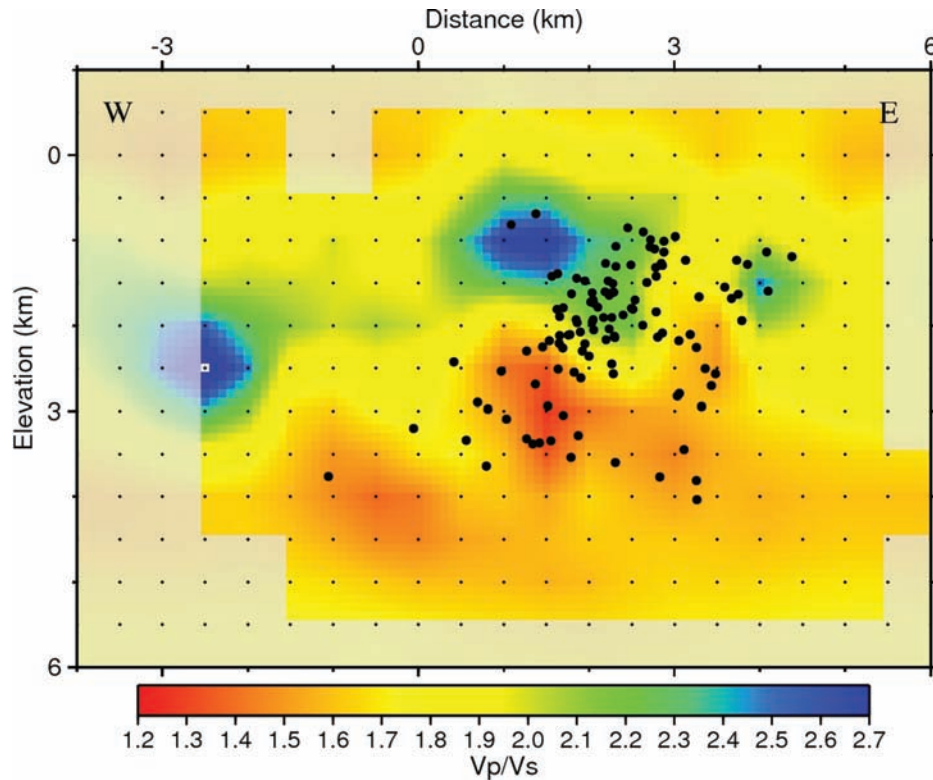
Figure 14 Tomography results: East-West cross-section at y=2500 of the Vp/Vs ratio.

anomaly, which extends from Capo Miseno in the West to the Island of Nisida in the East, with velocity values around 3500-4000 m/s as compared to values of 2500–3000 m/s for sediments filling the inner region of the Pozzuoli Bay. At approximately the same depth an anomalous high value of the Vp/Vs ratio is observed on the vertical cross-section, passing below the town of Pozzuoli (Fig. 14). According to Zollo *et al.* (2003) and Judenherc and Zollo (2004), we suggest that the annular velocity anomaly represents the buried trace of the southern rim of the Campi Flegrei caldera. The relatively high velocities of rocks forming the rim could be related to the presence of lava or tuff with inter-bedded lava according to stratigraphic and sonic logs inferred from deep boreholes (AGIP 1987). Deposits filling the inner bay area are instead characterized by relatively low Vp and high Vp/Vs values, which can be the evidence for a thick brine rock sedimentary layer (Vanorio *et al.* 2005). Recently, Dello Iacono *et al.* (submitted) analysed the P-to-P and P-to-S phases reflected from a very shallow seismic discontinuity at 500–700 m depth, detected by the seismic reflection analysis of data from a recent 3D active seismic survey (SERAPIS 2001). The move-out velocity analysis and stack of the P-P and P-S reflections at the layer bottom allowed them to estimate relatively high Vp/Vs values (3.5 ± 0.6). Based

on theoretical rock physical modelling of the Vp/Vs ratio as a function of porosity, the authors conclude that the shallow layer is likely formed by incoherent, water saturated, volcanic and marine sediments that filled Pozzuoli Bay during the post-caldera activity.

The buried caldera rim is well visible, also at greater depths from the obtained tomographic model. The section at 1.5 km depth (Fig. 13) allows one to roughly estimate a diameter of 10 km of the annular high Vp anomaly with a thickness of about 1 km. By comparing the tomographic image with Bouguer anomaly maps, based on data acquired in the early eighties (AGIP 1987; Barberi *et al.* 1991; Florio *et al.* 1999; Capuano and Achauer 2003) one can find a good correlation between the geometry and position of the velocity anomaly and the positive gravity anomaly, which has been attributed to the presence of hydrothermalized lava formations (Fig. 16), detected in Mofete wells at about 1 km depth. More recently, Tramelli *et al.* (2006) applied the scattering imaging method to coda waves of earthquake seismograms and were able to identify at 1–2 km depth the caldera border, behaving as a strong seismic signal scatterer with areas having the largest scattering coefficient nearly corresponding to the high Vp anomaly of this study. The mentioned observations along with results from

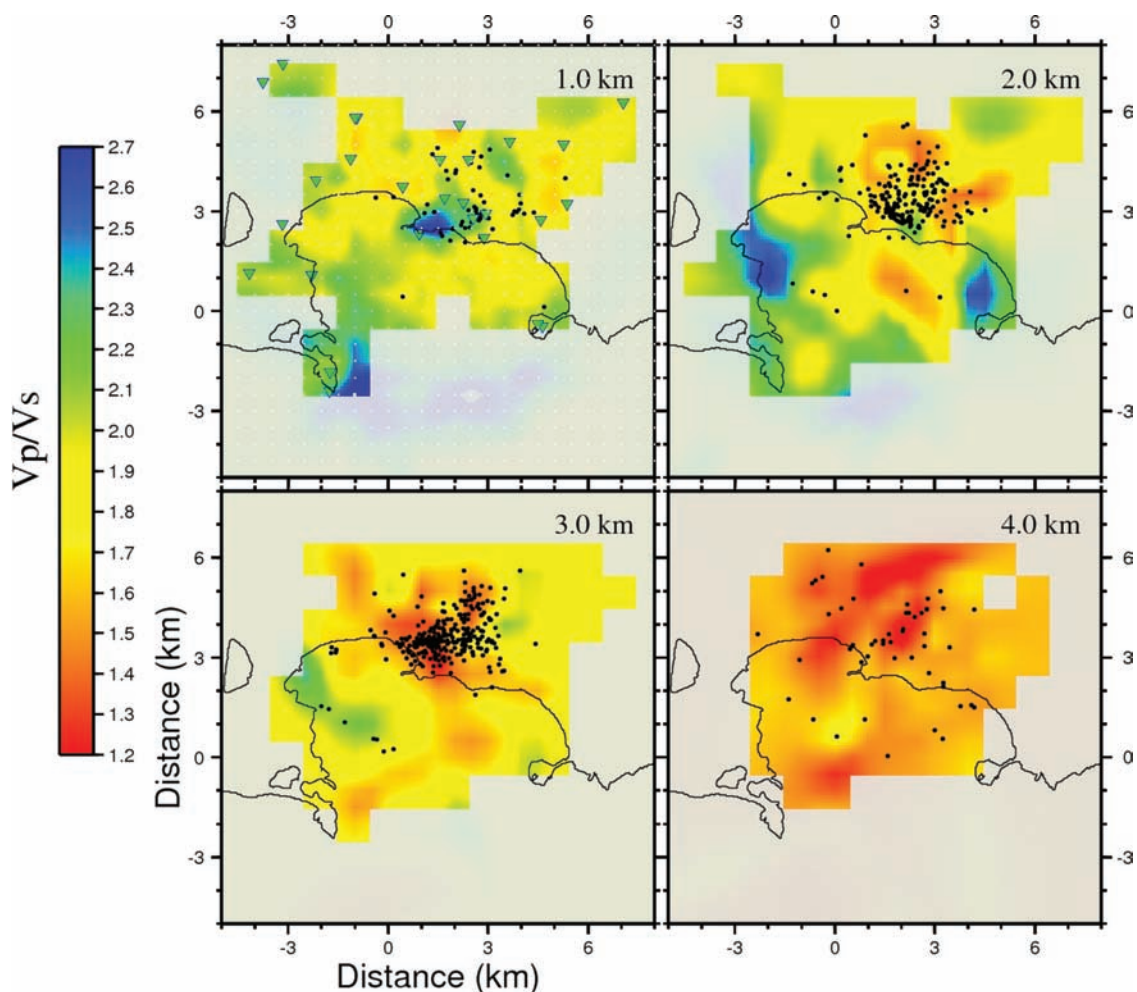**Figure 15** Tomography results: horizontal cross-sections of the Vp/Vs ratio.

the present study confirm the possible nature of the caldera rim, as formed by lithologies having higher density and velocity with respect to sequences which have filled the collapsed caldera region in the post-caldera period.

The annular Vp anomaly is still present at 3 km depth, although its diameter appears to reduce (Fig. 13). According to checkerboard resolution tests (Fig. 10) the ray coverage at this depth is sufficient to provide a good sampling of cells of the tomographic volume. Overall we can therefore estimate a sub-circular form for the Campi Flegrei caldera and an approximate rim elevation of 2 km. At about 4 km depth the annular Vp anomaly is no longer visible, corresponding with a sharp decrease of resolution at these depths for zones outside of Pozzuoli Bay. The tomographic Vp velocities of 5500 m/s are compatible with those of carbonatic rocks which likely form the deep basement of the caldera (Judenherc and Zollo 2004).

At 3–4 km depth the vertical tomographic sections of Vp/Vs confirm the presence of a low Vp/Vs body with values down to 1.3–1.4 extending below a large part of the caldera (Vanorio *et al.* 2005; Chiarabba and Moretti 2006). Earthquakes relocated in the 3D velocity model are distributed mostly at the top of this anomaly. The presence of liquid saturated rocks produces a decrease in rock compressibility and therefore an increase of Vp and Vp/Vs. On the other hand, in case of gas bearing rocks, the rock compressibility increases by producing a decrease of Vp, while the value of Vs should not vary, since S-waves propagate only through the rock matrix. Overall, one expects anomalous low values of the Vp/Vs ratio in case of gas saturated rock formations. According to the interpretation of Vanorio *et al.* (2005), the evidence for a low Vp/Vs value at 3–4 km depth excludes the presence of melted rocks and it is likely to be attributed to the presence of fractured overpressured gas-bearing formations.
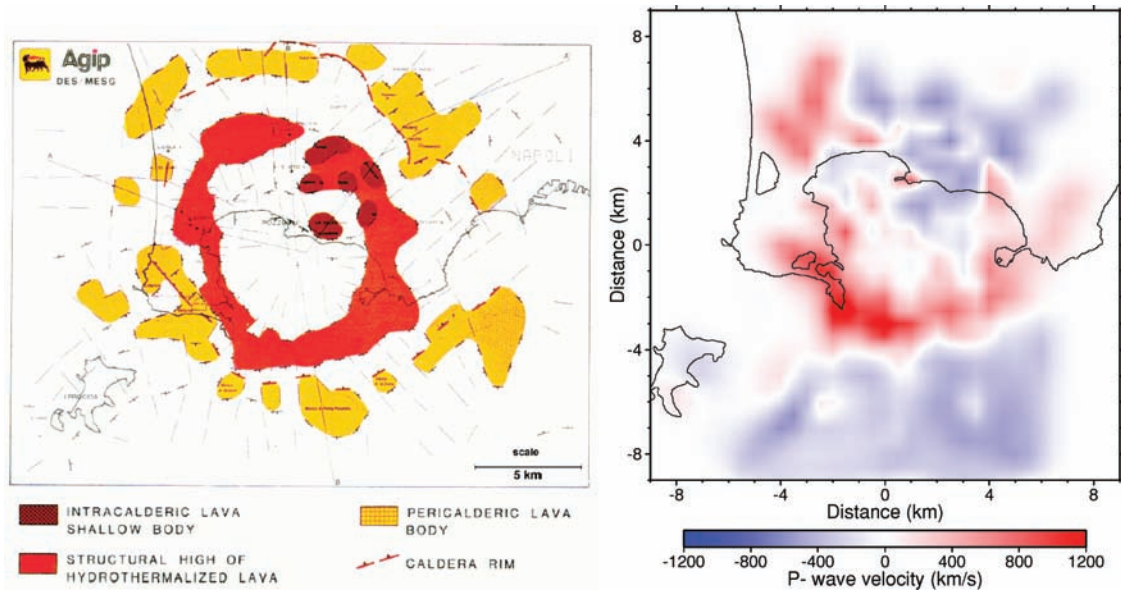
Figure 16 Left: 3D structure modeling of gravity observations (modified after AGIP 1987). Right: velocity anomaly at 1.5 km b.s.l. calculated as a difference between the final tomographic model and the initial mean 1D velocity model.
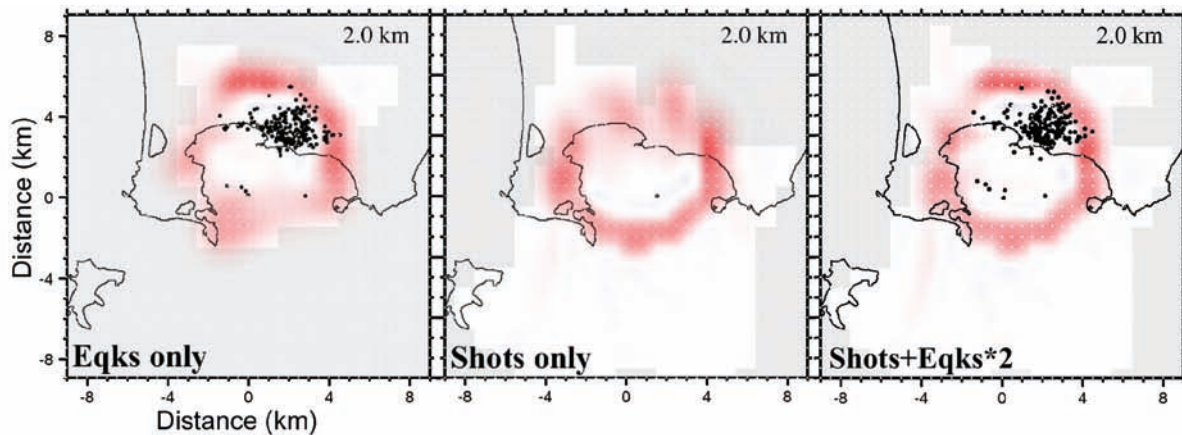

Figure 17 Reconstruction of P velocity anomaly (test T01) using earthquakes only (Eqks only), shots only and both with earthquake weights multiplied by 2.

CONCLUSIONS

By properly weighting the different data sets, we are able to optimally retrieve the information provided individually by both passive and active data. The merging of the two sets provides a single pair of P and S velocity models, which satisfies simultaneously all available traveltimes. The obtained improved resolution allows one to retrieve velocity anomalies over a large part of the tomography area in a more reliable way, as shown in Fig. 17, which compares the improved restitution of a synthetic anomaly with combined data sets to restitutions with individual sets.

The joint interpretation of the velocity distribution and Vp/Vs ratio together with the available gravity measurements and models, and the geothermal drilling information, has allowed us to locate and map lithological units at depth under the bay of Pozzuoli and under the inland portion of the Campi Flegrei. The shape of the caldera, whose rim was partially imaged at its southern border rim by Zollo *et al.* (2003) and Judenherc and Zollo (2004), is now integrally reconstructed both in its lateral and vertical extensions. This has been possible thanks to the efficient integration of earthquake and shot data which allows for a significant improvement of image resolution. The presence of the carbonatic bedrock underlying

the collapsed caldera structure, is confirmed by our study at about 4–5 km depth.

Results from the present study exclude the presence of a large magmatic body within the upper 5–6 km of the crust beneath the caldera. This calls into question previous hypotheses for the magma chamber depth at 4–5 km, based on earthquake locations, thermal data and sporadic observations of teleseismic records (Ferrucci *et al.* 1992). The evidence for a Mesozoic basement layer beneath the caldera, whose top occurs at a depth of 4–5 km, indicates that the magma chamber has to be well inside the limestone layer. The problems of identifying and locating the magma reservoir beneath Campi Flegrei caldera and investigating its connections to the deep Mt. Vesuvius feeding system have to be addressed by the analysis and modeling of reflection/conversion arrivals recorded during the SERAPIS experiment.

Our study confirms the presence of a low Vp/Vs anomaly at 4 km depth under the city of Pozzuoli, above which the earthquakes are located. This anomaly implies the presence of fractured, over-pressured, gas-bearing formations, and excludes the presence of melted rocks. At a shallow depth, a high Vp/Vs anomaly located at 1 km suggests the presence of rocks that contain fluids in the liquid phase. The modelling of the physical properties of the rock and the reversal trends encountered along velocity profiles leaded Vanorio *et al.* (2005) to interpret the low Vp/Vs anomaly at 4 km in depth as the top of formations that are enriched in gas that is under supercritical conditions. The 1982–1984 earthquake locations are mostly distributed on the top of velocity reversals and within the low Vp/Vs anomaly. Since these signatures were interpreted as being caused by gas under supercritical conditions, it can be speculated that the seismicity at Campi Flegrei caldera during unrests, is induced by over-pressured fluids. Further seismicity analysis has to be made with regard to this issue. Nevertheless, the phenomenological correlation among the uplift rate, the seismicity and the increase in the H_2O/CO_2 ratio in fumaroles as a function of time (Chiodini *et al.* 2001, 2003) would suggest that the observed phenomena may have a common origin.

ACKNOWLEDGEMENTS

REFERENCES

AGIP 1987. Geologia e geofisica del sistema geotermico dei Campi Flegrei. Servizi Centrali per l'Esplorazione, SERG-MMESG, San Donato.

Akaike H. 1974. A new look at the statistical model identification. *IEEE Transactions on Automatic Control* **19**, 716–723.

Aki K. and Lee W.H.K. 1976. Determination of three dimensional velocity anomalies under a seismic array using first P-arrival times from local earthquakes. *Journal of Geophysical Research* **81**, 4381–4399.

Aster R. and Meyer R. 1988. Three-dimensional velocity structure and hypocenter distribution in the Campi Flegrei caldera, Italy. *Tectonophysics* **149**, 195–218.

Barberi F., Corrado G., Innocenti F. and Luongo G. 1984. Phlegrean Fields 1982-1984: Brief chronicle of a volcano emergency in a densely populated area. *Bulletin of Volcanology* **47**, 175–185.

Barberi F., Cassano E., La Torre P. and Sbrana A. 1991. Structural evolution of Campi Flegrei caldera in light of volcanological and geophysical data. *Journal of Volcanology and Geothermal Research* **48**, 33–49.

Battaglia M., Troise C., Obrizzo F., Pingue F. and De Natale G. 2006. Evidence of fluid migration as the source of deformation at Campi Flegrei caldera (Italy). *Geophysical Resarch Letters* **33**, L01307. doi:10.1029/2005GL024904.

Benz H.M., Chouet B.A., Dawson P.B., Lahr J.C., Page R.A. and Hole J.A. 1996. Three-dimensional P and S wave velocity structure of Redoubt Volcano, Alaska. *Journal of Geophysical Research* **101**, 8111–8128.

Berrino G., Corrado G., Luongo G. and Toro B. 1984. Ground deformation and gravity changes accompanying the 1982 Pozzuoli uplift. *Bulletin of Volcanology* **47**, 187–200.

Bonafede M. 1991. Hot fluid migration: an efficient source of ground deformation: application to 1982-1984 crisis at Campi Flegrei, Italy. *Journal of Volcanology and Geothermal Research* **48**, 187–198.

Bonafede M. and Mazzanti M. 1998. Modeling gravity variations consistent with ground deformation in the Campi Flegrei caldera, Italy. *Journal of Volcanology and Geothermal Research* **81**, 137–157.

Capuano P. and Achauer U. 2003. Gravity field modeling in the Vesuvius and Campanian area. In: *TomoVes Seismic Project: Looking Inside Mt. Vesuvius* (eds A. Zollo, A. Bobbio, P. Gasparini, R. Casale and M. Yeroyanni). Cuen, Napoli.

Chiarabba C. and Moretti M. 2006. An insight into the unrest phenomena at the Campi Flegrei caldera from Vp and Vp/Vs tomography. *Terra Nova* **18**, 373–379.

Chiodini G., Frondini F., Cardellini C., Granieri D., Marini L. and Ventura G. 2001. CO2 degassing and energy release at Solfatara

volcano, Campi Flegrei, Italy. *Journal of Geophysical Research* **106**, 16213–16222.

Chiodini G., Todesco M., Caliro S., Del Gaudio C., Macedonio G. and Russo M. 2003. Magma degassing as a trigger of bradyseismic events: The case of Phlegrean Fields (Italy). *Geophysical Research Letters* **30**, 1434. doi:10.1029/2002GL016790.

Crosson R. 1976. Crustal structure modeling of earthquake data. 1. Simultaneous least square estimation of hypocenter and velocity parameters. *Journal of Geophysical Research* **81**, 3036–3046.

Dello Iacono D., Zollo A., Vassallo M., Vanorio T. and Judenherc S. 2007. Seismic image and rock properties of the very shallow structure of Campi Flegrei caldera (southern Italy). *Bulletin of Volcanology*, submitted.

Di Vito M.A., Lirer L., Mastrolorenzo G. and Rolandi G. 1987. The Monte Nuovo eruption (Campi Flegrei, Italy). *Bulletin of Volcanology* **49**, 608–615.

Dvorak J.J. and Berrino G. 1991. Recent ground movement and seismic activity in Campi Flegrei, Southern Italy: episodic growth of a resurgent dome. *Journal of Geophysical Research* **96**, 2309–2323.

Ferrucci F., Hirn A., de Natale G., Virieux J. and Mirabile L. 1992. P-SV conversions at a shallow boundary beneath Campi Flegrei caldera (Italy) - Evidence for the magma chamber. *Journal of Geophysical Research* **97**, 15351–15359.

Florio G., Fedi M., Cella F. and Rapolla A. 1999. The Campanian Plain and Campi Flegrei: structural setting from potential field data. *Journal of Volcanology and Geothermal Research* **91**, 361–379.

Gaeta S.G., De Natale G., Peluso F., Mastrolorenzo G., Castagnolo D., Troise C., Pingue F., Mita G. and Rossano S. 1998. Genesis and evolution of unrest episodes at Campi Flegrei caldera: the role of thermal fluid-dynamical processes in the geothermal system. *Journal of Geophysical Research* **103**, 20921–20933.

Gaeta F.S., Peluso F., Arienzo I., Castagnolo D., De Natale G., Milano G., Albanese C. and Mita D.G. 2003. A physical appraisal of a new aspect of bradyseism: The miniuplifts. *Journal of Geophysical Research* **33**, 2363. doi:10.1029/2002JB001913.

Gottsman, J., Rymer H. and Berrino G. 2006. Unrest at the Campi Flegrei caldera (Italy): A critical evaluation of source parameters from geodetic data inversion. *Journal of Volcanology and Geothermal Research* **150**, 132–145.

Judenherc S. and Zollo A. 2004. The Bay of Naples (Southern Italy): Constraints on the volcanic structures inferred from a dense seismic survey. *Journal of Geophysical Research* **33**, B10312.

Kissling E., Ellsworth W. L., Eberhart-Phillips D. and Kradolfer U. 1994. Initial reference models in local earthquake tomography. *Journal of Geophysical Research* **99**, 19635–19646.

Latorre D., Virieux J., Monfret T., Monteiller V., Vanorio T., Got J.-L. and Lyon-Caen H. 2004. A new seismic tomography of Aigion area (Gulf of Corinth-Greece) from a 1991 dataset. *Geophysical Journal International* **159**, 1013–1031.

Le Meur H., Virieux J. and Podvin P. 1997. Seismic tomography of the Gulf of Corinth: A comparison of methods. *Annales Geophysicae* **40**, 1–25.

Lee W.H.K. and Lahr J.C. 1975. HYPO71 (revised): A computer program for determining hypocenter, magnitude, and first motion pattern of local earthquakes. US Geological Survey Open File Report 75–311.

Monteiller V. 2005. Tomographie ál'aide de décalages temporels d'ondes sismiques P : développements méthodologiques et applications. PhD thesis, Université de Savoie.

Newhall C.G. and Dzurizin D. 1988. Historical unrest at large calderas of the world. *US Geological Survey Bulletin* **33**, 1108.

Orsi G., de Vito S. and Di Vito M. 1996. The restless, resurgent Campi Flegrei nested caldera (Italy): Constraints on its evolution and configuration. *Journal of Volcanology and Geothermal Research* **74**, 179–214.

Orsi G., Civetta L., Del Gaudio C., de Vita S., Di Vito M.A., Isaia R., Petrazzuoli S.M., Ricciardi G.P. and Ricco C. 1999. Short-term ground deformations and seismicity in the resurgent Campi Flegrei caldera (Italy): An example of active block-resurgence in a densely populated area. *Journal of Volcanology and Geothermal Research* **91**, 415–451.

Paige C.C. and Saunders M.A. 1982. LSQR: An algorithm for sparse linear equations and sparse least squares. *ACM Transactions on Mathematical Software* **8**, 43–71.

Podvin P. and Lecomte I. 1991. Finite difference computation of traveltimes in very contrasted velocity models: A massively parallel approach and its associated tools. *Geophysical Journal International* **105**, 271–284.

Scandone R., Bellucci F., Lirer L. and Rolandi G. 1991. The structure of the Campanian plain and the activity of the Napolitan volcanoes. *Journal of Volcanology and Geothermal Research* **48**, 1–31.

Schneider J., Aster R., Powell L. and Meyer R. 1987. Timing of portable seismographs from Omega navigational signals. *Bulletin of the Seismological Society of America* **77**, 1457–1478.

Spakman W. and Nolet G. 1988. Imaging algorithms, accuracy and resolution. In: *Mathematical Geophysics*M (ed.N. Vlaar), pp. 155–187. Springer.

Tarantola A. and Valette B. 1982. Generalized nonlinear inverse problems solved using the least-squares criterion. *Reviews of Geophysics and Space Physics* **20**, 219–232.

Thurber C.H. 1992. Hypocenter-velocity structure coupling in local earthquake tomography. *Physics of the Earth and Planetary Interiors* **75**, 55–62.

Tramelli A., Del Pezzo E., Bianco F. and Boschi E. 2006. 3D scattering image of the Campi Flegrei caldera (Southern Italy). *Physics of the Earth and Planetary Interiors* **155**, 269–280.

Troise C., De Natale G., Pingue F., Obrizzo F., De Martino P., Tammaro U. and Boschi E. 2007. Renewed ground uplift at Campi Flegrei caldera (Italy): New insight on magmatic processes and forecast. *Geophysical Research Letters* **33**, L03301. doi:10.1029/2006GL028545.

Vanorio T., Virieux J., Capuano P. and Russo G. 2005. Three-dimensional seismic tomography from P wave and S wave microearthquake traveltimes and rock physics characterization of the Campi Flegrei Caldera. *Journal of Geophysical Research* **33**, B03201. doi:10.1029/2004GL003102.

Zollo A., Judenherc S., Auger E., D'Auria L., Virieux J., Capuano P., Chiarabba C., de Franco R., Makris J., Michelini A. and Musacchio G. 2003. Evidence for the buried rim of Campi Flegrei caldera from 3-d active seismic imaging. *Geophysical Research Letters* **33**. doi:10.1029/2003GL018173.